FEBS Letters 582 (2008) 3776–3782

# Robustness analysis of cellular memory in an autoactivating positive feedback system

Zhang Cheng, Feng Liu*, Xiao-Peng Zhang, Wei Wang*

*National Laboratory of Solid State Microstructure and Department of Physics, Nanjing University, Nanjing 210093, China*

Received 19 February 2008; revised 26 September 2008; accepted 6 October 2008

Available online 16 October 2008

Edited by Robert B. Russell

**Abstract** **Cellular memory is a ubiquitous phenomenon in cell biology. Using numerical simulation and theoretical analysis, we explored the robustness of cellular memory to intrinsic noise in a transcriptional positive feedback system. Without noise, the system could create two stable steady states and function as a memory module. Memory robustness index and mean first-passage time were used to quantify the robustness of memory. Large cell size and strong cooperativity in binding enhanced memory storage remarkably. Adding a second positive feedback loop improved persistent memory significantly, whereas including a negative one destabilized memory storage. These are consistent with experimental observations. We interpret why positive feedback loops are actively involved in epigenetic memory from a dynamical systems perspective.**



*Keywords:* Cellular memory; Autoactivating positive feedback system; Robustness analysis; Cell size; Cooperativity in binding; Interlinked feedback loop

## 1. Introduction

Cells are identified according to their characteristic patterns of gene expression and silencing [1,2]. Information can be passed from one generation to another not only in the form of genome sequence but also in expression patterns of genes. The latter, called epigenetic cellular memory, involves transient signals locking cells into one of two or more regulatory states. These states should be stable over time and may be inherited through cell division. Epigenetic memory is important to various cellular processes such as metabolism, development, and circadian rhythms [3,4].

One of the simplest mechanisms for cellular memory is based on positive feedback loops [5,6], which are ubiquitous and play important roles in cellular signaling [7]. Such loops with some ultrasensitivity are considered sufficient to create two stable states [5,8]. Transitions between alternative states exhibit hysteresis or even irreversibility, and thus the loop can function as a memory module [5,9]. For example, it keeps Xenopus oocytes mature even after the steroid hormone progesterone is removed [6,9]. It is also involved in the uptake of nutrition molecules in bacteria [10,11]. Moreover, this module is one of building blocks in synthetic biology and has significant implications for biotechnology, biocomputing and gene therapy [12–16].

Since chemical reactions are essentially probabilistic and reactants such as genes, RNAs and proteins are present in low numbers per cell, intrinsic noise is inevitable and has various influences on cellular signaling [17,18]. Noise may drive a bistable system to undergo stochastic transitions between alternative states, which may impair memory storage [13]. However, robustness — the ability to maintain reliable functions despite external and internal perturbations — is a long-recognized key property of living systems [19]. A memory module must sustain the states induced by transient signals over a timescale like the cell-cycle period. On the other hand, although theoretical analysis of autoactivating positive feedback systems has been performed [20,21], little work has addressed the issue of how cellular memory is robust to noise from a dynamical systems perspective. Thus, it is intriguing to explore cellular mechanisms for persistent memory by using numerical simulation and theoretical analysis.

In this Letter we investigated the robustness of cellular memory to intrinsic noise in the context of an autoactivating positive feedback system. Both deterministic and stochastic models were constructed to describe the dynamics of the system. Without noise, the system could create two stable steady states and function as a memory module. We used two measures, i.e., memory robustness index and mean first-passage time, to quantify memory storage. It is demonstrated that large cell size and strong cooperativity in binding can greatly enhance memory storage. Moreover, adding a second positive feedback loop enhances persistent memory significantly, whereas introducing a negative one destabilizes memory storage evidently. These are in agreement with experimental observations. Our results suggest that cells are capable of sustaining persistent memory via various mechanisms.

## 2. Materials and methods

An autoactivating positive feedback loop is one of the simplest circuits able to exhibit multiple stable states [5,6]. The circuit is composed of a single gene encoding a transcription factor (TF-A), which activates its own transcription when bound to specific responsive-element (TF-RE) DNA sequence (Fig. 1A). The binding has a cooperative effect [8], which was quantified by Hill function. The degradation of TF-A was modeled as a first-order process with a rate constant $k_{deg}$, while the basal rate for the synthesis of TF-A was $R_{bas}$.

As a result, the deterministic dynamics of the model were described by the following rate equation [13,22]:

*Corresponding authors. Fax: +86 25 83595535.
*E-mail addresses:* fliu@nju.edu.cn (F. Liu), wangwei@nju.edu.cn (W. Wang).

0014-5793/$34.00 
doi:10.1016/j.febslet.2008.10.005

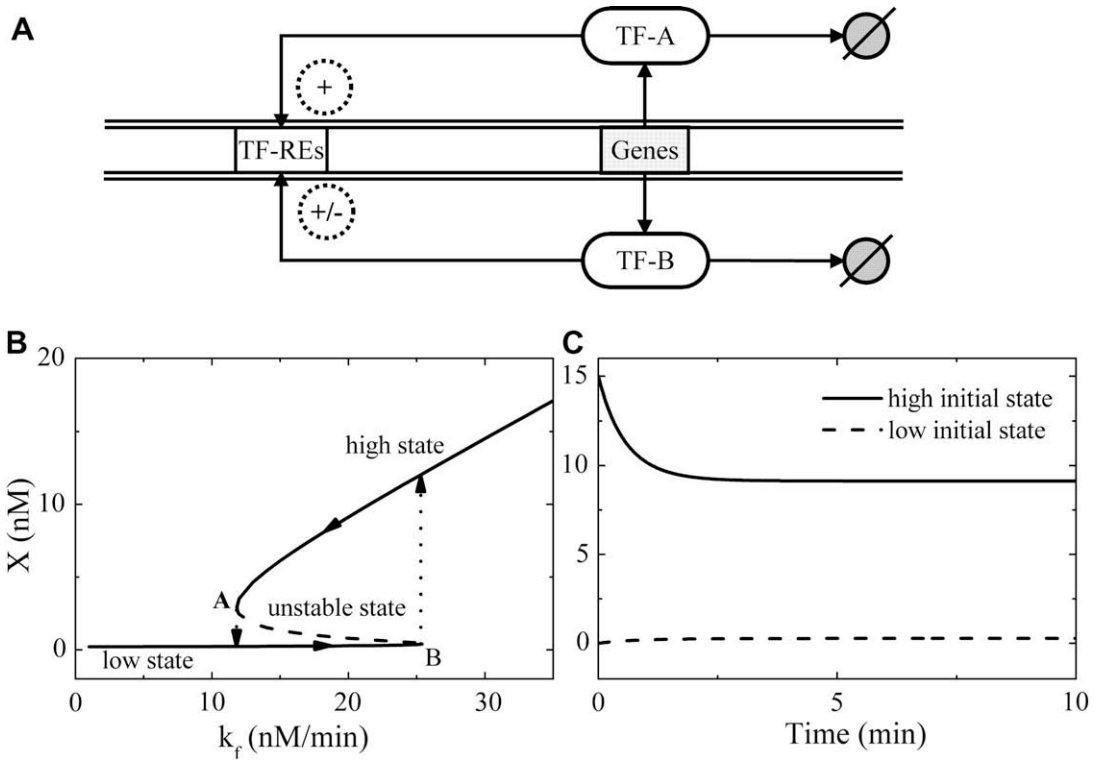


Fig. 1. The model and bifurcation diagram. (A) Schematics of the model for genetic regulation in an autoactivating feedback loop (only the upper half) together with a second positive ('+') or negative ('−') feedback loop. (B) Bifurcation diagram for the deterministic dynamics. Two saddle-node bifurcation points, $k_f^{\mathrm{A}} = 11.82$ and $k_f^{\mathrm{B}} = 25.41$, enclose a memory region. (C) History-dependent behavior. With the same stimulus ($k_f = 20$), two systems with different initial states (separately at the high and low states) still keep their states separate over time.

$$\frac{dx}{dt} = \frac{k_f x^n}{x^n + K_{\mathrm{d}}} - k_{\mathrm{deg}} x + R_{\mathrm{bas}}, \tag{1}$$

where $x$ denotes the concentration of TF-A, $K_{\mathrm{d}}$ is the dissociation constant of TF-A from TF-RE, and $n$ represents the cooperativity in binding. The maximum transcription rate $k_f$ is a key control parameter indicating stimulus level. The parameter values used were as follows: $K_{\mathrm{d}} = 10\ \mathrm{nM}^n$, $R_{\mathrm{bas}} = 0.4\ \mathrm{nM\ min}^{-1}$, $k_{\mathrm{deg}} = 2\ \mathrm{min}^{-1}$, and $n = 2$ unless otherwise specified.

When only a small number of proteins and individual copies of the target gene are involved, the above deterministic description is no longer appropriate owing to intrinsic stochasticity of chemical reactions, which generally can be described by birth-and-death stochastic processes governed by chemical master equations. For simplicity, here we considered the model composed of two parallel processes, $N \to N+1$ and $N \to N-1$, running separately with the rates [23]

$$W_1(N) = \left(R_{\mathrm{bas}} + \frac{k_f N^n}{N^n + K_{\mathrm{d}} V^n}\right) V, \tag{2}$$

$$W_2(N) = k_{\mathrm{deg}} N. \tag{3}$$

$N$ is the number of TF-A molecules and $V$ is cell size. The corresponding master equation was written as follows:

$$\frac{\partial P(N,t)}{\partial t} = W_1(N-1)P(N-1,t) + W_2(N+1)P(N+1,t) - (W_1(N) + W_2(N))P(N,t), \tag{4}$$

where $P(N,t)$ is the probability distribution at time $t$. We performed stochastic simulations by using the Gillespie algorithm [24].

On the other hand, we performed theoretical analysis by converting the master equation into the Fokker–Planck equation, which was given by

$$\frac{\partial P(x,t)}{\partial t} = -\frac{\partial}{\partial x} A(x) P(x,t) + \frac{1}{2V} \frac{\partial^2}{\partial x^2} B(x) P(x,t), \tag{5}$$

with

$$A(x) = \frac{k_f x^n}{x^n + K_{\mathrm{d}}} - k_{\mathrm{deg}} x + R_{\mathrm{bas}} \tag{6}$$

$$B(x) = \frac{k_f x^n}{x^n + K_{\mathrm{d}}} + k_{\mathrm{deg}} x + R_{\mathrm{bas}}. \tag{7}$$

We solved for its steady state distribution, obtaining

$$P_s(x) = C e^{-2V\phi(x)}, \tag{8}$$

where $C$ is a normalization constant. The stochastic potential $\phi(x)$ was described as [25]

$$\phi(x) = \frac{1}{2V} \ln\left(\frac{B(x)}{2V}\right) - \int_0^x \frac{A(s)}{B(s)} ds. \tag{9}$$

$\phi(x)$ provides an intuitive representation of the stability of steady states [10].

When noise is present in bistable systems, there is always a chance that a perturbation will flip the system from one steady state to the other. Thus, a quantity of interest is the time elapsed until the system flips from one initial state to the other for the first time, which is referred to as the first-passage time [20]. Here we presented results for the mean first-passage time (MFPT), which theoretically satisfies the following equation [20]:

$$-1 = A(x)\frac{dT(x)}{dx} + \frac{B(x)}{2V}\frac{d^2T(x)}{dx^2}. \tag{10}$$

We also considered the impact of cell growth on memory storage. During growth, cell size could be explicitly described as $V(t) = V_0 \exp(k_g t)$ with $k_g = \ln 2/T_c$, where $V_0$ is the initial size and $T_c$ is the period of cell-cycle [23]. Here $T_c$ sets the timescale for studying the systems's memory effect. We used the following values: $T_c = 20$ h and $V_0 = 30\ \mathrm{nM}^{-1}$; the constant cell size was set to $30\ \mathrm{nM}^{-1}$ unless otherwise specified. Given the cell size is $30\ \mathrm{nM}^{-1}$, the corresponding cell volume is about $50\ \mu\mathrm{m}^3$.

Moreover, interlinked feedback loops are frequently found in bistable systems, and a detailed list of such biological systems can be found in Refs. [26,27]. Thus, it is intriguing to explore the effect of interlinked

feedback loops on memory storage. To this end, we introduced a second negative or positive feedback loop in the model (see the loop containing TF-B in Fig. 1A). After adding the negative feedback loop, we described the dynamical equations of the interlinked system as follows [28]:

$$\frac{dx}{dt} = k_f\left[\frac{x^n}{x^n + K_d}\right]\left[\frac{K_{d,y}}{y^n + K_{d,y}}\right] - k_{deg}x + R_{bas} \quad (11)$$

$$\frac{dy}{dt} = k_{f,y}\left[\frac{x^n}{x^n + K_d}\right]\left[\frac{K_{d,y}}{y^n + K_{d,y}}\right] - k_{deg,y}y + R_{bas,y}. \quad (12)$$

After adding the positive feedback loop, we had

$$\frac{dx}{dt} = k_f\left[\frac{x^n}{x^n + K_d} + \frac{y^n}{y^n + K_{d,y}}\right] - k_{deg}x + R_{bas} \quad (13)$$

$$\frac{dy}{dt} = k_{f,y}\left[\frac{x^n}{x^n + K_d} + \frac{y^n}{y^n + K_{d,y}}\right] - k_{deg,y}y + R_{bas,y}. \quad (14)$$

$k_{f,y}$ determines the feedback strength in the second loop [28]. The parameter values were as follows: $K_{d,y} = 15\ \mathrm{nM}^n$, $R_{bas,y} = 0.05\ \mathrm{nM\ min^{-1}}$, and $k_{deg,y} = 1\ \mathrm{min^{-1}}$.

## 3. Results

The autoactivating positive feedback system can display bistability over a wide range of stimulus strength $k_f$. Fig. 1B shows the bifurcation diagram for the deterministic model as a function of $k_f$. Two saddle-node bifurcation points, $k_f^A = 11.82\ \mathrm{nM\ min^{-1}}$ and $k_f^B = 25.41\ \mathrm{nM\ min^{-1}}$, enclose a bistable region. For any $k_f$ within this regime, the system has two stable steady states at low and high concentrations and an unstable steady state at intermediate values. When moving rightwards along the lower stable branch by increasing $k_f$ until $k_f^B$, the system remains in the low state. When moving leftwards along the upper stable branch by decreasing $k_f$ until $k_f^A$, the system remains in the high state. Therefore, the state of the system is not only determined by present conditions but also depends on the path by which the present state has been reached, i.e., it is history-dependent (see Fig. 1C as an example). In this study, memory refers to history-dependent behaviors, and the bistable regime is also called memory region [29].

Since the number of reactants involved in the system is small, we should take into account intrinsic noise. In the following, we explore the robustness of cellular memory to noise and identify potential mechanisms for enhancing it.

We first investigate noise-induced transitions between alternative steady states. Suppose that an individual system is subjected to a stimulus with the strength in the memory region (e.g., $k_f = 13.5$) and is initially in the low steady state, i.e., there are few activators available. Fig. 2A illustrates its three typical behaviors over the time interval from 0 to $T_c$: (1) it is trapped in the initial state and there is no transition; (2) it flips from the low to high state and remains there; (3) it is first driven to the high state and then back to the low state. These behaviors occur with different probabilities. In this case, the first behavior occurs most frequently, whereas the others occur sparsely. As transitions happen, the memory of the initial state is disrupted. Here we explore whether the steady state of the system is kept up to the cell-cycle period $T_c$.

Since the states of individual systems vary greatly from case to case, it is necessary to consider the population dynamics and to characterize memory storage in terms of statistical distributions. To this end, we assume that a population of 4000 cells containing this loop is simultaneously driven by the same stimulus. We record the state of the population by calculating a histogram of the number $N$ of TF-A molecules at $T_c$. Here history-dependent behaviors refer to a good separation of distributions for different initial conditions [10].

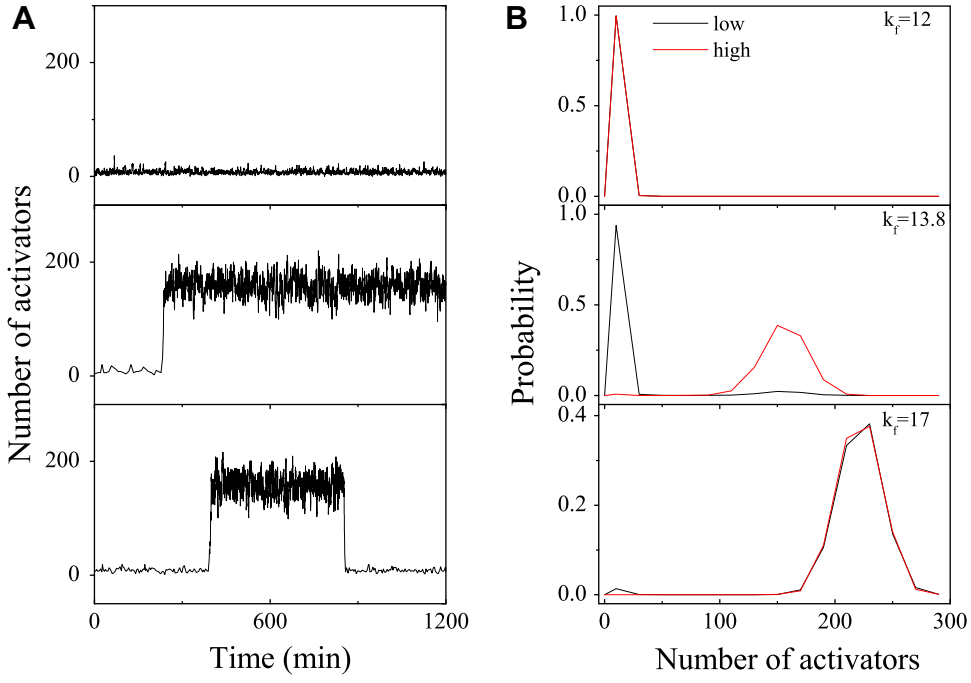


Fig. 2. The dynamics of systems in the presence of noise. (A) Sample traces of $N(t)$ for different noise realizations with $k_f = 13.5$. (B) Histograms for $N(T_c)$ with $k_f = 12$, 13.8, and 17 (from top to bottom). Black and red lines separately represent that all systems are initially in the low and high steady states for $k_f$ in the deterministic case. The size bin is 20.

Fig. 2B depicts the histograms for two different initial conditions. When $k_f$ is around the lower threshold (e.g., $k_f = 12$), the two histograms converge to the same distribution, which is sharply centered at the low state. Similarly, for $k_f = 17$ the two histograms nearly converge to the same distribution, which is mostly centered around the high state. That is, in these cases the final distribution is history-independent, and thus the memory is lost. In contrast, for $k_f = 13.8$ the two histograms are well separated, with one sharply centered at the low state and the other mostly centered around the high state. That is, the system basically displays a persistent memory of the initial state. Thus, the degree to which the memory is robust to noise depends remarkably on $k_f$.

Two measures were used to quantify memory storage. One is memory robustness index, $\Gamma_{MRI}$, which is defined as the area of non-overlapping section between the two histograms with the size bin being 1. Thus, $\Gamma_{MRI}$ is between 0 and 1. The memory of initial state is most robust to noise when $\Gamma_{MRI} = 1$ and lest robust when $\Gamma_{MRI} = 0$. This measure is consistent with experimentally measuring the distributions for the number of proteins by using fluorescent method [10]. The other is the mean first-passage time (MFPT). The longer MFPT, the more stable the state. There are two steady states in the model, and the MFPT for the transition from the low to high state and that for the opposite transition are separately denoted by $\tau_L$ and $\tau_H$. Any frequent transitions in either direction will destabilize memory.

Fig. 3A displays $\Gamma_{MRI}$ versus $k_f$. When cell size is fixed, $\Gamma_{MRI}$ takes a relatively large value when $13.5 \leqslant k_f \leqslant 15.3$ and is close to 0 when $k_f > 17$. It has a maximum around $k_f = 13.8$, i.e., there is an optimal stimulus strength for maintaining persistent memory.

The MFPT as a function of $k_f$ is shown in Fig. 3B, where the MFPT is compared with $T_c$. There exist two critical values, $k_f^C = 13.0$ and $k_f^D = 15.6$, where $\tau_H$ and $\tau_L$ are equal to $T_c$, respectively. When $k_f$ is between the critical values, both $\tau_H$ and $\tau_L$ are larger than $T_c$. Especially, for $k_f = 13.8$ $\tau_H$ equals $\tau_L$ and is far larger than $T_c$. Large value of the MFPT means a low possibility for transitions between alternative states over the timescale of $T_c$. Thus, the range between $k_f^C$ and $k_f^D$ defines a persistent memory regime. When $k_f$ is beyond this range, either $\tau_L$ or $\tau_H$ is larger than $T_c$. As a result, the memory is destabilized by noise. Note that the simulation results are in perfect agreement with the theoretical data derived from Eq. 10, as the simulation points fall on the solid lines in Fig. 3B.

We can interpret the above dependence of two measures on $k_f$ in terms of stochastic potential $\phi$ [see Eq. 9]. Fig. 3C displays the potential landscapes for different values of $k_f$, where two local minima correspond to steady states that are separated by an energy barrier. Driven by noise with sufficient intensity, the system can flip from one steady state to the other across the barrier. The model has two energy barriers corresponding to transitions in two directions, respectively. Generally, the larger the energy barrier, the more efficiently the fluctuations in states are trapped around the steady states. The barrier height depends remarkably on $k_f$. For $k_f = 12$, the high state becomes metastable compared to the low state, and thus the transition from the high to low state can easily happen. Indeed, in this case $\tau_L$ is three orders of magnitude larger than $T_c$, whereas $\tau_H$ is only 25 min. Similarly, for $k_f = 17$ the low state becomes metastable, while the high state has a far larger energy barrier. In the above cases, one steady state is easily destabilized. In contrast, for $k_f = 13.8$ the two steady states are nearly of the same relatively large energy barriers. Thus, both states are resistant to noise.

In brief, we can characterize the robustness of memory in terms of $\Gamma_{MRI}$ and the MFPT. The two measures are consistent with each other. They show the same optimality range for memory storage. But this range is narrow compared with the whole memory regime. This implies that the autoactivating

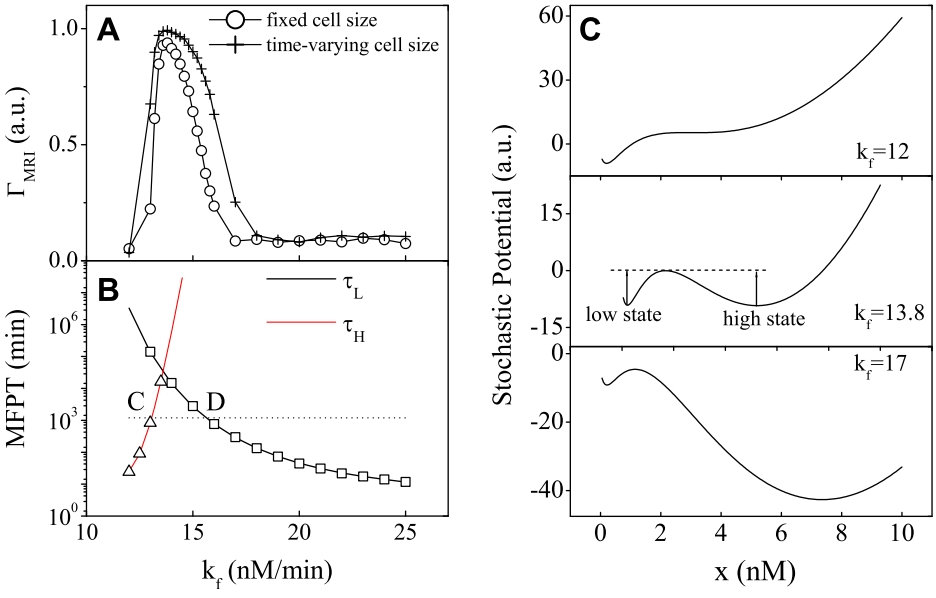


Fig. 3. Quantifying the robustness of cellular memory to noise. (A) $\Gamma_{MRI}$ as a function of $k_f$ when cell size is fixed (○) or varies temporally (+). There exists a persistent memory regime around $k_f = 13.8$. (B) The MFPT for the transition from the low to the high state (□) or vice versa (△) vs. $k_f$. The dotted line marks the period of cell cycle ($T_c$). The solid lines are theoretical results derived from Eq. 10. There are two critical points, $k_f^C = 13.0$ and $k_f^D = 15.6$, where the MFPT is equal to $T_c$. The range between $k_f^C$ and $k_f^D$ defines a persistent memory regime. (C) The stochastic potential vs. the concentration of TF-A for different values of $k_f$.

positive feedback system with $n = 2$ acts as a robust memory module only operating on a narrow parameter range. To produce persistent memory over a wider parameter range, other cellular mechanisms should be exploited. In the following, we investigate the effects of cell growth, cell size, cooperativity in binding, and a second feedback loop on memory storage in terms of $\Gamma_{MRI}$.

When cells grow from $V_0 = 30$ to $V = 60$ at $T_c$, the memory region is slightly widened (data not shown) and the capacity of storing the initial state is improved. The persistent memory region is also enlarged, while $\Gamma_{MRI}$ is close to 1 around $k_f = 13.8$ (Fig. 3A, the curve with cross). This implies that cell growth acts as a dilution to the intrinsic noise and subserves memory storage. But this effect depends remarkably on the initial value $V_0$.

For simplicity, we keep the cell size constant on individual trials and systematically explore the effect of cell size on memory storage. Fig. 4 displays $\Gamma_{MRI}$ versus $k_f$ as a function of cell size. As $V$ increases, the memory regime becomes wide and $\Gamma_{MRI}$ increases. Accordingly, the persistent memory region is enlarged, where $\Gamma_{MRI}$ is closer to 1. For large cell size (e.g., $V = 150$), $\Gamma_{MRI}$ is 1 over a wide range of $k_f$ (broader than half of the memory region). This occurs because the noise intensity is proportional to $1/\sqrt{V}$ [18]. As a result, weak noise is associated with large cells, and cellular memory is enhanced by effectively decreasing stochastic transitions. For sufficiently large cells, the intrinsic noise is so weak that the loop behaves like operating in the deterministic case, and $\Gamma_{MRI}$ is 1 over the whole memory region.

Now we turn to consider the effect of cooperative binding, which is characterized by $n$ in the Hill function, on memory storage. It has been demonstrated that any degree of cooperativity ($n > 1$) in positive feedback loops is sufficient for the emergence of bistability [5,8]. In our model, strong cooperativity can remarkably improve memory storage (Fig. 5). For $n = 4$, the system can keep a perfect memory of initial states with $\Gamma_{MRI}$ close to 1 over the whole range shown. In fact, larger $n$ increases both the energy barriers and the separation of two local minima in the potential landscape, causing transitions between alternative states more difficult to occur.

Finally, we explore the effect of a second negative or positive feedback loop on memory storage. As seen in the bifurcation diagram (Fig. 6A), when the strength $k_{f,y}$ of negative feedback

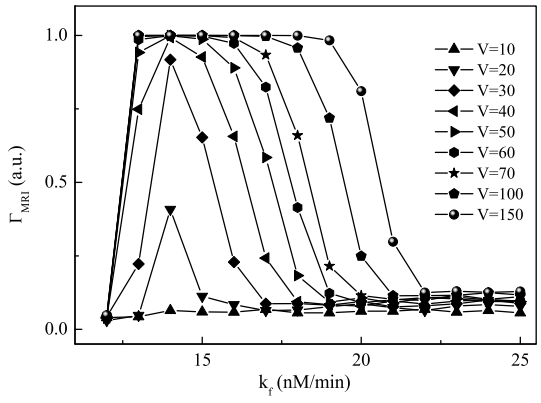


Fig. 4. Effect of cell size on memory storage. $\Gamma_{MRI}$ as a function of $k_f$ for different values of cell size. Evidently, memory storage is greatly enhanced with large cell size.

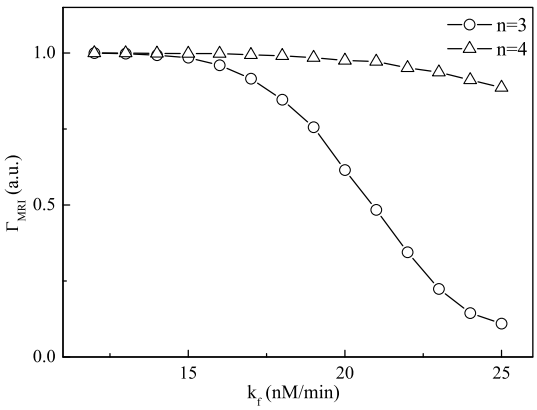


Fig. 5. $\Gamma_{MRI}$ vs. $k_f$ for $n = 3$ (○) and $n = 4$ (△), respectively. Strong cooperativity in binding can enhance memory storage remarkably.

is increased from 0 to 5, the lower threshold increases but the higher threshold is nearly fixed. Meanwhile, the values of high steady state also decrease. Thus, the memory region is narrowed with increasing $k_{f,y}$. Accordingly, the maximum of $\Gamma_{MRI}$ greatly drops, while the persistent memory region is remarkably reduced (Fig. 6C). That is, the negative feedback destabilizes memory storage. In contrast, a positive feedback loop promotes memory storage. When $k_{f,y}$ is increased from 0 to 5, the lower threshold is decreased from 11.8 to 4.4, while the higher threshold changes slightly (Fig. 6B). That is, the memory region is remarkably widened. Meanwhile, the values of high steady state are amplified. The region over which $\Gamma_{MRI}$ is close to 1 is greatly enlarged (Fig. 6D). Thus, adding a positive feedback loop can enhance persistent memory significantly.

We can interpret the above differences in terms of energy potential landscape. The negative feedback tends to decrease the energy barriers, and thus the probability for random transitions between alternative states is greatly increased. In contrast, the positive feedback tends to increase the distance between two local minima, which makes noise-induced transitions harder to occur.

Our results are also consistent with the experimental observations in the galactose signaling pathway of budding yeast, where persistent memory is maintained by a core positive feedback loop through Gal3p [10]. This memory is further enhanced by a positive feedback loop mediated by Gal2p but is destabilized by a negative feedback loop through Gal80p. These results suggest that cells may exploit interlinked feedback loops to control memory storage.

## 4. Discussion

In this work, we have investigated the robustness of cellular memory in the context of an autoactivating positive feedback system. We used two measures to quantify memory storage and found that large cell size, strong cooperativity in binding, and a second positive feedback loop can promote memory storage. These indicate that cells can develop various mechanisms to ensure persistent memory.

Large cell size and strong cooperativity in binding have previously been reported to subserve the robustness of circadian rhythms [30,31]. Moreover, Gonze et al. have found that in circadian systems the robustness of rhythms to noise is enhanced

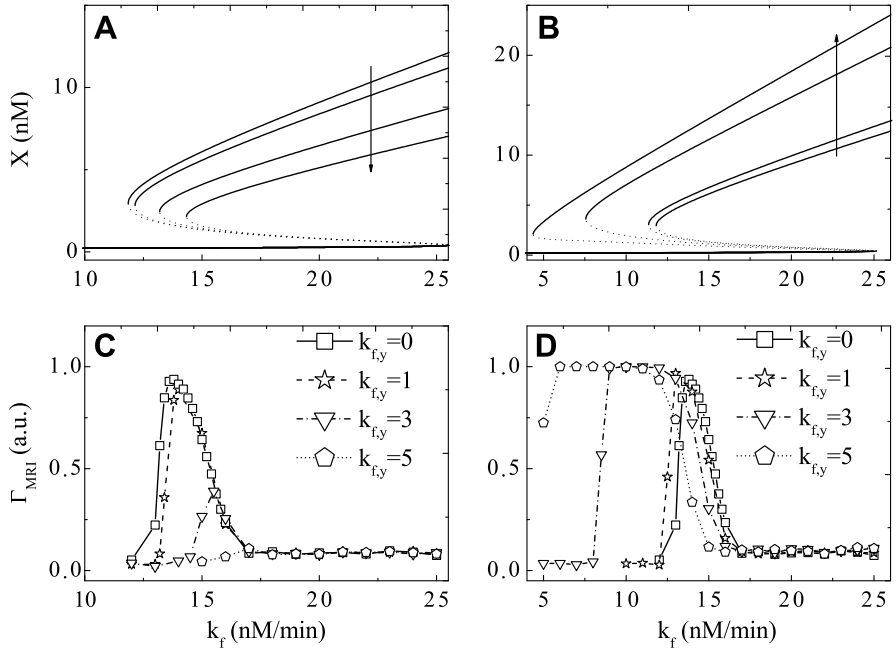


Fig. 6. Effect of a second negative (A, C) or positive (B, D) feedback loop on memory storage. (A–B) Bifurcation diagram for the deterministic interlinked loops. The arrow in the panels indicates that the value of $k_{f,y}$ increases from 0, 1, 3, to 5. (C–D) $\Gamma_{MRI}$ vs $k_f$ for different feedback strength.

as the distance away from the bifurcation point increases [30]. In our model, there are two bifurcation points, and there is an optimal stimulus strength intermediate within the memory region. These imply that cells may exploit a same set of mechanisms to perform various functions.

It has been demonstrated that interlinked fast and slow positive feedback loops can act as an optimal switch [26,32]. Here we found that interlinked positive feedback loops can improve memory storage and that negative feedback loops destabilize memory. These results are consistent with the experimental observations [10]. Kim et al. have also analyzed the robustness of memory in mutual inhibitory positive feedback loop (MIPF) [29]. They found that interlinked MIPF systems can realize more robust cellular memory compared to single MIPFs. However, their measure of robustness is only the area of the memory region, a static variable. The dynamics of the system in response to perturbations have not been described. In contrast, we have depicted the dynamics of the system in detail and identified the mechanisms for persistent memory.

It is worth comparing our work with two recent papers [20,21], which explored the effect of noise from various sources on the dynamics of a positive feedback loop system. Kepler and Elston considered two sources of intrinsic noise (i.e., small number of molecules and slow operator fluctuations) [20], while Mantzaris further distinguished extrinsic noise (i.e., unequal partitioning of cellular material at cell division) from intrinsic noise [21]. Both papers investigated the effect of various noise on the width of the bistability region but did not explicitly describe the effect of cell size on system dynamics. Kepler and Elston also discussed the stability of low steady state in terms of the MFPT. However, robustness of cellular memory is different from stability of steady states, since the former refers to the ability to maintain persistent memory of initial state over time despite noise. It is insufficient to explore memory storage only based on the analysis of the bistability region. Here we took intrinsic stochasticity of chemical reactions as the source of intrinsic noise and explored its effect on memory storage. We investigated whether cell population dynamics exhibit history-dependent behaviors on the time interval from 0 to $T_c$. We calculated $\Gamma_{MRI}$ or the MFPT for transitions in both directions, and only when $\Gamma_{MRI}$ is close to 1 or both $\tau_L$ and $\tau_H$ are larger than $T_c$ can we verify that cellular memory is robust to noise. Thus, only by analyzing system dynamics in that way can we uncover the mechanisms for persistent memory based on bistability.

Since cellular memory is important to various cellular functions and intrinsic noise is inevitable inside cells, the robustness of memory storage to noise is vital to living systems. Our findings provide new insights into how perfect memory can be implemented via ubiquitous mechanisms and may also be helpful to design optimal memory modules in synthetic biology. Our findings further verify that an autoactivating positive feedback system is a key regulatory motif with the capacity of realizing epigenetic memory.

*Acknowledgement:* This work was supported by the National Basic Research Program of China (Grant No. 2007CB814806) and the NNSF of China (Grant No. 10604028).

## References

[1] Orlando, V. (2003) Polycomb, epigenomes, and control of cell identity. Cell 112, 599–606.
[2] Turner, B.M. (2002) Cellular memory and the histone code. Cell 111, 285–291.
[3] Casadesús, J. and D'Ari, R. (2002) Memory in bacteria and phage. Bioessays 24, 512–518.
[4] Wolf, D.M. and Arkin, A.P. (2003) Motifs, modules and games in bacteria. Curr. Opin. Microbiol. 6, 125–134.
[5] Ferrell, J.E. (2002) Self-perpetuating states in signal transduction: positive feedback, double-negative feedback and bistability. Curr. Opin. Cell Biol. 14, 140–148.

[6] Xiong, W. and Ferrell, J.E. (2003) A positive-feedback-based bistable 'memory module' that governs a cell fate decision. Nature 426, 460–465.
[7] Freeman, M. (2000) Feedback control of intercellular signalling in development. Nature 408, 313–319.
[8] Cherry, J.L. and Adler, F.R. (2000) How to make a biological switch. J. Theor. Biol. 203, 117–133.
[9] Ferrell, J.E. and Xiong, W. (2001) Bistability in cell signaling: how to make continuous processes discontinuous, and reversible processes irreversible. Chaos 11, 227–236.
[10] Acar, M., Becskei, A. and van Oudenaarden, A. (2005) Enhancement of cellular memory by reducing stochastic transitions. Nature 435, 228–232.
[11] Ozbudak, E.M., Thattai, M., Lim, H.N., Shraiman, B.I. and van Oudenaarden, A. (2004) Multistability in the lactose utilization network of *Escherichia coli*. Nature 427, 737–740.
[12] Gardner, T.S., Cantor, C.R. and Collins, J.J. (2000) Construction of a genetic toggle switch in *Escherichia coli*. Nature 403, 339–342.
[13] Becskei, A., Séraphin, B. and Serrano, L. (2001) Positive feedback in eukaryotic gene networks: cell differentiation by graded to binary response conversion. EMBO J. 20, 2528–2535.
[14] Hasty, J., McMillen, D. and Collins, J.J. (2002) Engineered gene circuits. Nature 420, 224–230.
[15] Arkin, A.P. (2001) Synthetic cell biology. Curr. Opin. Biotech. 12, 638–644.
[16] Alon, U. (2007) Network motifs: theory and experimental approaches. Nat. Rev. Genet. 8, 450–461.
[17] Rao, C.V., Wolf, D.M. and Arkin, A.P. (2002) Control, exploitation and tolerance of intracellular noise. Nature 420, 231–237.
[18] Kaern, M., Elston, T.C., Blake, W.J. and Collins, J.J. (2005) Stochasticity in gene expression: from theories to phenotypes. Nat. Rev. Genet. 6, 451–464.
[19] Stelling, J., Sauer, U., Szallasi, Z., Doyle, F.J. and Doyle, J. (2004) Robustness of cellular functions. Cell 118, 675–685.
[20] Kepler, T.B. and Elston, T.C. (2001) Stochasticity in transcriptional regulation: Origins, consequences, and mathematical representations. Biophys. J. 81, 3116–3136.
[21] Mantzaris, N.V. (2007) From single-cell genetic architecture to cell population dynamics: quantitatively decomposing the effects of different population heterogeneity sources for a genetic network with positive feedback architecture. Biophys. J. 92, 4271–4288.
[22] Smolen, P., Baxter, D.A. and Byrne, J.H. (1998) Frequency selectivity, multistability, and oscillations emerge from models of genetic regulatory systems. Am. J. Physiol. 274, C531–C542.
[23] Zhdanov, V.P. (2006) Transient stochastic bistable kinetics of gene transcription during the cellular growth. Chem. Phys. Lett. 424, 394–398.
[24] Gillespie, D.T. (1977) Exact stochastic simulation of coupled chemical reactions. J. Phys. Chem. 81, 2340–2361.
[25] Risken, H. (1984) The Fokker–Planck Equation, Springer, Berlin.
[26] Brandman, O., Ferrell, J.E., Li, R. and Meyer, T. (2005) Interlinked fast and slow positive feedback loops drive reliable cell decisions. Science 310, 496–498.
[27] Kim, D., Kwon, Y.K. and Cho, K.H. (2007) Coupled positive and negative feedback circuits form an essential building block of cellular signaling pathways. Bioessays 29, 85–90.
[28] Song, H., Smolen, P., Av-Ron, E., Baxter, D.A. and Byrne, J.H. (2007) Dynamics of a minimal model of interlocked positive and negative feedback loops of transcriptional regulation by cAMP-response element binding proteins. Biophys. J. 92, 3407–3424.
[29] Kim, T.H., Jung, S.H. and Cho, K.H. (2007) Interlinked mutual inhibitory positive feedbacks induce robust cellular memory effects. FEBS Lett. 581, 4899–4904.
[30] Gonze, D. and Goldbeter, A. (2006) Circadian rhythms and molecular noise. Chaos 16, 026110.
[31] Gonze, D., Halloy, J. and Goldbeter, A. (2002) Robustness of circadian rhythms with respect to molecular noise. Proc. Natl. Acad. Sci. USA 99, 673–678.
[32] Zhang, X.P., Cheng, Z., Liu, F. and Wang, W. (2007) Linking fast and slow positive feedback loops reates an optimal bistable switch in cell signaling. Phys. Rev. E 76, 031924.